Western U.S. Seismic Anisotropy Revealing Complex Mantle Dynamics

Quan Zhou[a], Jiashun Hu[a], Lijun Liu[a,*], Thomas Chaparro[b], Dave Stegman[b], Manuele Faccenda[c]

a. Department of Geology, University of Illinois at Urbana-Champaign, Urbana, IL, 61801, USA

b. IGPP, Scripps Institution of Oceanography, UC San Diego, La Jolla, CA, 92093, USA

c. Dipartimento di Geoscienze, Università di Padova, 35131, Padova, Italy

* Corresponding author's email address: ljliu@illinois.edu (L. Liu).

Abstract

The origin of the complex pattern of SKS splitting over the western United States (U.S.) remains a long-lasting debate, where a model that simultaneously matches the various SKS features is still lacking. Here we present a series of quantitative geodynamic models with data assimilation that systematically evaluate the influence of different lithospheric and mantle structures on mantle flow and seismic anisotropy. These tests reveal a configuration of mantle deformation more complex than ever envisioned before. In particular, we find that both lithospheric thickness variations and toroidal flows around the Juan de Fuca slab modulate flow locally, but their co-existence enhances large-scale mantle deformation below the western U.S. The ancient Farallon slab below the east coast pulls the western U.S. upper mantle eastward, spanning the regionally extensive circular pattern of SKS splitting. The prominent E-W oriented anisotropy pattern within the Pacific Northwest reflects the

existence of sustaining eastward intrusion of the hot Pacific oceanic mantle to beneath the continental interior, from within slab tears below Oregon to under the Snake River Plain and the Yellowstone caldera. This work provides an independent support to the formation of intra-plate volcanism due to intruding shallow hot mantle instead of a rising mantle plume.

1. Introduction

Seismic anisotropy, the directional dependence of seismic wave speed, is a strong constraint on mantle flow. Upper mantle seismic anisotropy is usually attributed to the lattice-preferred orientation (LPO) of olivine, the most abundant mineral in the upper mantle (Karato et al., 2008). When upper mantle rocks are subject to deformation in the dislocation regime, mineral grains develop an LPO by dislocation creep, dynamic recrystallization, and grain-boundary migration (Karato and Wu, 1993; Kaminski et al., 2004), leading to macroscopic seismic anisotropy. In nature, the development of seismic anisotropy can be further affected by water content (Jung and Karato, 2001; Katayma and Karato, 2006), pressure (Couvy et al., 2004; Durinck et al., 2005; Raterron et al., 2009), differential stress (Karato et al., 2008), and temperature (Katayma and Karato, 2006). While the formation of mantle anisotropy likely involves multiple processes, it has been suggested that olivine fast axis tends to align with the maximum shear direction for a simple mantle flow (Zhang and Karato, 1995; Long and Becker, 2010).

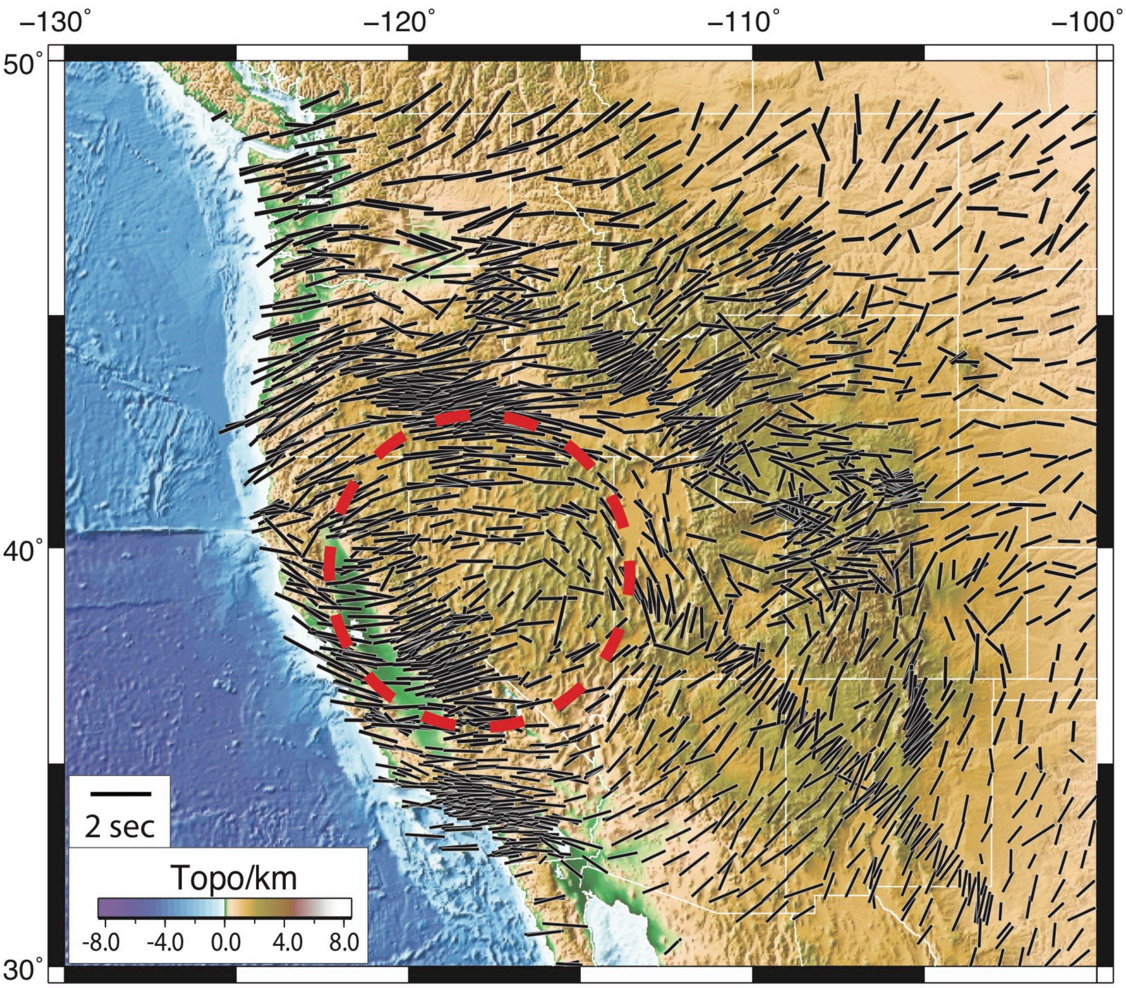

Figure 1: SKS observation (Becker et al. 2012) and topography (ETOPO1.0) over the western U.S. Key anisotropy features include the fast SKS splitting from Oregon to Wyoming, the large scale circular pattern centered in western Nevada, and the sharp anisotropy transition along the lithospheric step in Wyoming and Utah. SRP: Snake River Plain, RM: Rocky Mountains, NBR: Northern Basin & Range, SBR: Southern Basin & Range, CP: Colorado Plateau.

The observed seismic anisotropy via shear wave splitting (SWS) over the western United States (U.S.), however, demonstrates a very complex spatial pattern (Fig. 1, Wüstefeld et al., 2009; Becker et al., 2012). In contrast to the commonly observed trench-normal or trench-parallel directions (Long, 2016), SWS (mostly SKS measurements) in the western U.S. demonstrates systematic spatial variations (Fig. 1). Along the coast, from ~40° N northward toward Washington (WA), the fast direction rotates from largely SW-NE to E-W; this trend reverses going southward where the fast direction quickly switches to NW-SE in central California (CA) and to E-W in southern CA and northern Mexico. Moving inland to the back-arc region, all fast directions rotate to a quasi E-W direction, including those from WA to southern CA. The anisotropy reaches the highest magnitude in southeastern Oregon (OR) and southwestern Idaho (ID), with the delay time reaching 2 seconds (Long, 2016). Further inland, to the south of the Snake River Plain (SRP), the spatial rotation continues from that on the west, forming a broad circular pattern centered in western Nevada (NV) and a secondary circle in northernmost CA. To the north of the OR-NV border, the fast direction remains largely E-W into west Montana (MT) and Wyoming (WY), where the thin western U.S. lithosphere transitions into thick cratonic lithosphere to the east. In between the north and the south, the fast direction follows the province boundaries of SRP eastward to the Yellowstone (YS) volcanic field in WY.

Besides SWS, there are also seismic observations constraining the depth-dependence of mantle anisotropy, including those based on body waves (Huang and Zhao, 2013; Buehler and Shearer, 2014), surface waves (Beghein et al., 2010; Yuan and Romanowicz ,2010; Lin et al., 2011; Wagner et al., 2013; Wagner and Long, 2013), receiver functions (Park et al., 2004; Nikulin et al., 2009), and Love-to-Rayleigh wave scattering (Rieger and Park, 2010). However, these other results, likely due to their different methodology and sensitivity, demonstrate relatively low consistency for the depth-dependent anisotropy below the region. Consequently, a direct comparison of these observations with geodynamic modeling is not conclusive.

The complex SWS pattern in the western U.S. has led to different interpretations of the underlying mantle dynamics. Zandt and Humphreys (2008) attributed the large circular pattern to toroidal flow around the southern edge of the Juan de Fuca slab. West et al. (2009) proposed a model of lithospheric drip below the Great Basin as the cause of the circular SWS pattern. Druken et al. (2011) suggested that mantle flow induced by slab rollback generates the E-W fast direction beneath Oregon and Idaho. These models either focus on part of the observations, or only represent a conceptual model. To reconcile these potential debates, we attempt to better constrain the origin of the complex anisotropy pattern by developing a data-oriented mantle flow model for North America during the last 20 million years (Ma). The mantle flow model matches multiple key observational constraints simultaneously, including past plate motion, Basin & Range (B&R) deformation, present-day mantle structure (Zhou and Liu, 2017) and the time-dependence of intra-plate volcanisms within the western U.S. (Zhou et al. 2018). Based on these geodynamic models, we then analyze the effects of different mantle structures on the formation of seismic anisotropy including both LPO and SWS, using an approach similar to our recent study over South America (Hu et al., 2017).

2. Data and Methods

The method for calculating seismic anisotropy consists of two steps: 1) Reconstruction of mantle thermal evolution and associated mantle flow since 20 Ma.

2) Converting the mantle flow history to seismic anisotropy (LPO) and synthetic SWS (SKS) measurements.

2.1 Reconstructing past mantle flow

We adopt the hybrid data assimilation approach for mantle convection, as described with more details in Zhou and Liu (2017), to simulate mantle flow below continental U.S. during the last 20 Ma. Here we provide a brief summary of the approach. The hybrid data assimilation consists of two parts: forward and adjoint data assimilations. In the forward part, we assimilate a recent plate reconstruction (Müller et al., 2008) as the velocity boundary condition. We also use the reconstructed seafloor ages to update the temperature structure of the oceanic lithosphere. The model viscosity is both depth- and temperature-dependent. Lateral viscosity variations also include weak mantle wedge near the subduction zone that allows the reproduction of fine-scale slab evolution and mantle flow (Zhou and Liu, 2017). The initial condition of the forward model only assimilates the subducting oceanic slab, without including the various mantle structures imaged in seismic tomography (Sigloch, 2011; Schmandt and Lin, 2014). To solve this problem, we then use the adjoint data assimilation to further incorporate these other features (Zhou and Liu, 2017).

For the adjoint part of the model, the reference present-day mantle structure is based on a merged image of two recent high-resolution tomography models (Schmandt and Lin, 2014; and Sigloch, 2011). We use Schmandt and Lin (2014) to define the fine-scale structure below the U.S. and use Sigloch (2011) to approximate regions beyond, with a smooth transition along their boundaries. More details about the construction of the reference thermal state could be found in Zhou and Liu (2017). During the hybrid assimilation approach, mismatches from the forward integration of mantle evolution could be corrected through subsequent adjoint integrations, which iteratively update the initial condition (Zhou and Liu, 2017). Compared to our earlier adjoint approach (Liu and Gurnis, 2008), the hybrid approach further assimilates seafloor age as an additional input, producing finer slab structures than outlined by tomography. Together, this new model better represents various dynamic structures (Fig. 2) affecting mantle evolution below the western U.S. since 20 Ma (Zhou and Liu, 2017).

In practice, we implemented the hybrid data assimilation approach into the open source mantle convection code CitcomS (Zhong et al., 2008). We performed 32 hybrid iterations until the solution converges. Thus derived mantle evolution provides a new explanation for the origin of the western U.S. volcanic history by showing that majority of the underlying heat source was from the Pacific upper mantle instead of from the putative Yellowstone plume (Zhou et al., 2018). Here we use this mantle flow model as one end-member scenario to better understand the nature of the complex seismic anisotropy in the region. To quantify the effects of various mantle structures, we perform additional simulations where we focus on the resulting mantle flow with different combinations of these mantle structures: 1) continental lithosphere with laterally varying thickness, 2) subducting Juan de Fuca slab since 20 Ma, 3) ancient Farallon slabs below central-eastern U.S., and 4) hot mantle anomalies associated with intraplate volcanisms.

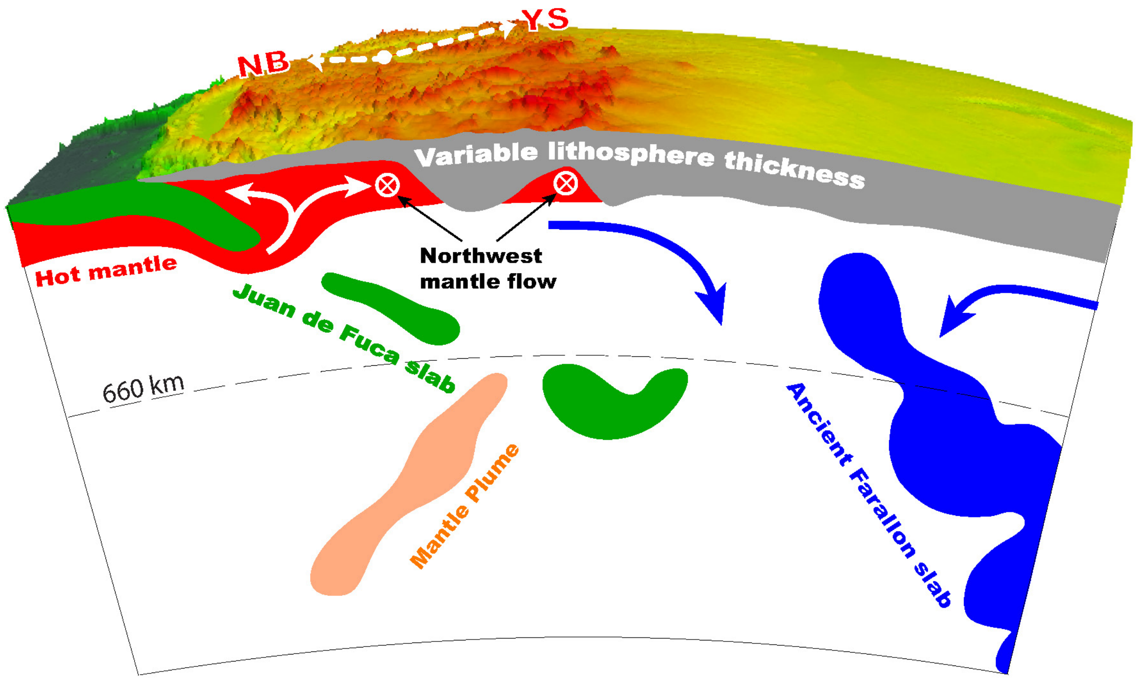

Figure 2: A summary of mantle structures below the U.S. that are responsible for driving mantle flow. These features, all based on the tomography of Schmandt & Lin (2014) and Sigloch (2011), include 1) a variable lithosphere thickness, 2) the actively subducting Juan de Fuca slab below the western U.S., 3) the still descending ancient Farallon slab below central-eastern U.S., 4) recently identified eastward encroaching hot Pacific mantle to underneath the thin western U.S. lithosphere, and 5) a southwestward tilted mantle plume in the lower mantle (Nelson & Grand, 2018).

Relative to the published models (e.g., Zhou et al., 2018), the models presented here include one more structural feature: a small-scale (~200 km in diameter) fast anomaly currently extending to ~200 km depth below central Nevada (Fig. 3a, 3b; Schmandt and Lin, 2014), previously interpreted as a lithospheric drip (West et al., 2009; Schmandt and Humphreys, 2010). We emphasize that this feature is not the same as that assumed in West et al. (2009) who interpreted a continuous upper-mantle scale fast anomaly as a lithospheric drip. Due to both limited resolution of our numerical model and the large amount of extension within the B&R (McQuarrie and

Wernicke, 2005), this fast anomaly is difficult to simulate prior to 10 Ma when NV state was half of its present width. Dynamically, this small feature does not influence the regional-scale mantle flow, but it does affect flow surrounding it and thus the local anisotropy pattern. Therefore, we assimilate this feature at 8 Ma in all models so that it better matches the present seismic image.

2.2 Calculating mantle anisotropy and SKS splitting

In order to simulate the formation of LPO, we adopt a similar approach to that of Kaminski et al. (2004) that considers the effects of dislocation creep, dynamic recrystallization, and grain-boundary migration. Our LPO simulator is a recently updated FORTRAN software DRexS (Hu et al., 2017), a high-performance parallel code tailored for mantle flow in spherical coordinates, extended from 3D-DRex (Faccenda and Capitanio, 2013).

The simulation starts with a large number of Lagrangian particles representing mineral aggregates, with 50 km horizontal spacing and 30 km vertical spacing. The mineral aggregates assume 70% A-type olivine and 30% enstatite. The particles have random orientation initially, which results in an isotropic mantle. With the mantle flow imposed, the particles change orientations based on the mechanisms mentioned above and start to form macroscopic anisotropy. The output is the full elastic tensor associated with the particles. The upper mantle is dominated by transverse isotropy, and, therefore, the symmetry axis of the transverse isotropy, i.e. TI axis, outlines the structure of the elastic tensor. For most aggregates, the modeled LPO is such that the TI axis coincides with the olivine fast axis (OFA) (Faccenda and Capitanio, 2013).

We perform the above procedure for all the mantle flow models generated, and then compute their SWS prediction with the output full elastic tensors. We use the software package FSTRACK (Becker et al., 2006) to generate the synthetic SKS. This code employs full waveform modeling incorporating finite frequency effects. It reads in the elastic tensors output from DRexS. Then it computes synthetic seismograms by assuming an incident plane wave into the mantle over a range of frequencies (0 – 5 Hz) via inverse Fourier transform. The incident wave has a ray incidence of 5°, typical for SKS arrivals. After that, the code bandpass-filters the seismograms from 0.05 to 0.3 Hz to be consistent with real SKS measurements. A cross-correlation method (Menke and Levin, 2003) is then used to compute the splitting time from the synthetic seismograms, taking the average of the SKS apparent splitting parameters measured as a function of backazimuth (e.g., Becker et al., 2006, EPSL). We also vary the amount of time over which mantle flow is applied, and we find that a 10-Ma history provides the best anisotropy result, although with limited improvement in predicted anisotropy compared to a longer time window (e.g., 20 Ma).

3. Results

In this section, we present the predictions of mantle flow, OFA, and resulting SKS splitting from the five different mantle models described in section 2.1. We start with the simplest case where only the effect of the lithosphere thickness variation is considered. Then we gradually add in other tectonic structures including the Juan de Fuca slab, the ancient Farallon slab, and the hot mantle anomalies, respectively.

3.1 Model 1: Variable lithospheric thickness

Mantle flow modulated by lithospheric thickness variation represents a commonly proposed mechanism for seismic anisotropy (Assumpção et al., 2006; Wang et al., 2008; Foster et al., 2014). Here we test the effect of the seismically inferred lithospheric structure on mantle flow pattern subject to the observed plate motion history. For a lithosphere with uniform thickness, its movement over a low-viscosity asthenosphere would form the typical Couette flow, where the flow direction parallels that of the surface plate and the flow speed decreases with depth. This has been proposed as the mechanism to form plate motion-parallel seismic anisotropy (Vinnik et al., 1992; Fouch et al., 2000; Becker et al., 2014; Hu et al., 2017). Lithospheric thickness variations, especially that along the direction of plate motion, could modify mantle flow and thus change the pattern of seismic anisotropy (e.g., Wang et al., 2008; Foster et al., 2014).

For the western U.S., the plate motion since 20 Ma has been largely westward (e.g., Müller et al., 2008). The lithosphere is thin throughout most of the western U.S., with a rapid increase in thickness to the east of the Rockies into the cratonic interior (Hansen et al., 2015). This thickness variation is also revealed in both body-wave (e.g., Schmandt and Lin, 2014) and surface wave tomography (e.g., Shen and Ritswoller, 2016). In our calculation, for the cratonic region to the east, we take the upper 200 km cold anomalies as representing the continental lithosphere. In the active tectonic region, there is no lithosphere according to the tomography adopted (Schmandt and Lin, 2014), as is due to the lack of vertical resolution of body wave inversion. Consequently, this tends to over-estimate the effect of lithospheric thickness variation on diverting mantle flow (Fig. 3a, 3b).

The resulting mantle flow largely displays a plate-motion-driven pattern, both in the oceanic and continental regions. Down to 200 km depth, the oceanic mantle mostly follows the surface plate velocity (Fig. 3a, 3b). One exception is the narrow, young Juan de Fuca-plate, where the mantle flow, especially at >100 km depths, is strongly affected by the fast motion of the Pacific plate to the west and the south. Within the continent, mantle flow below the craton area inherits the surface motion due to the thick strong lithosphere. In contrast, the mantle below the tectonic region on the west, where lithosphere is thin, deviates from the surface velocity to flow slightly southward. The change of flow direction below the western U.S. likely reflects the effect of the lithospheric step that largely orients NW-SE, favoring a southward flow diversion.

The predicted mantle anisotropy displays different patterns across the subduction zone. In the oceanic mantle, the OFAs at different depths are consistent with surface plate motion (Fig. 3c-3d), a result similar to that in Hu et al. (2017). On the continental side, the interior of the thick cratonic lithosphere (<200 km depth) has no LPO fabrics developed (Fig. 3c), indicating little shear deformation inside the strong lithosphere. At greater depths (Fig. 3d), the anisotropy below the craton displays little change over depths, mostly parallel with plate motion. The OFAs below the tectonic region, delineated by the lithospheric step, differ significantly from the direction of plate motion. A narrow zone of anomalous NW-SE oriented OFAs closely follows the strike of the lithospheric step below 200 km depth. This is a result of shear deformation along this boundary, where the mantle to the west feels less mechanical entrainment from above, as also seen from the change in mantle velocity. In NV, the mantle flow

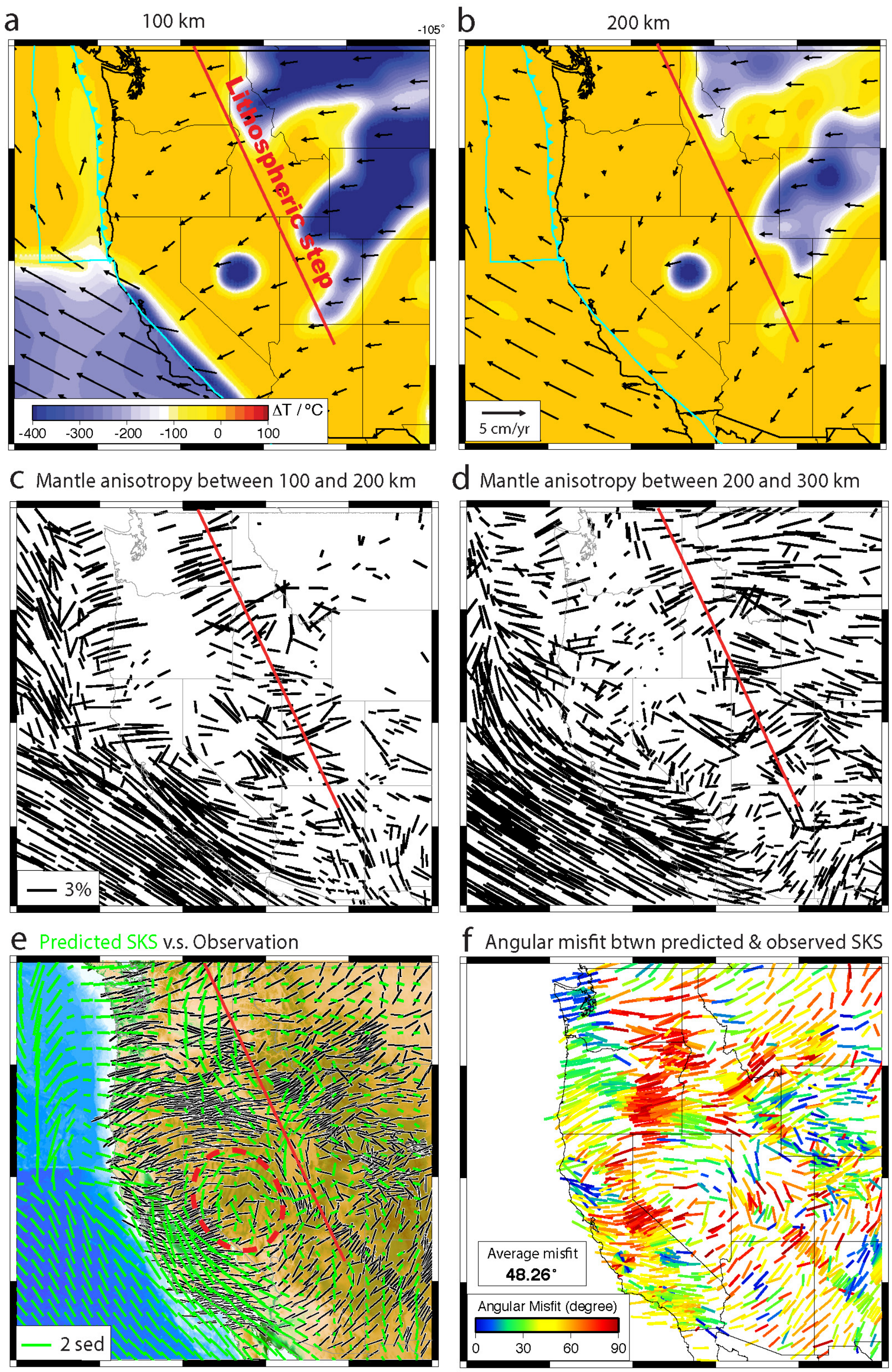

Figure 3: Mantle flow and anisotropy prediction from Model 1 at present-day. (a-b) Temperature and mantle flow at two different depths. The red line approximates the location of the sharp thickness increase of the North American lithosphere from west to east. (c-d) Modeled mantle anisotropy, represented by the

TI axis, at two different depth ranges. (e) Predicted (green) and observed (black) SKS splitting. The red dashed circle outlines a local swirl pattern predicted by the model. (f) Distributed angular misfit and its regional average of the predicted and observed SKS patterns.

is locally diverted around the central cold anomaly, and this generates a radial pattern of OFAs above ~300 km (Fig. 3c, 3d). In CA, the OFAs are roughly parallel to the coast (Fig. 3c-d), implying shear deformation near the continental boundary where the E-W plate motion transitions into NW-SE in the Pacific. The obviously different spatial patterns of mantle velocity and LPO suggest that the former is a poor approximation of seismic anisotropy for tectonically active regions.

The predicted SKS (Fig. 3e) has a strong dependence on the depth distribution of LPO (Fig. 3c-d). In the regions where the LPO patterns are consistent over depth, such as the ocean basin, the coast area, the craton region, and southern B&R, the SKS prediction aligns well with OFAs at depths. In regions where anisotropy patterns vary with depth, like NV, the correlation with SKS is reduced. In comparison with the observed SKS, prediction from Model 1 fails to match most of the features within the western U.S. (Fig. 3e-f), with a regionally averaged angular misfit being as much as 48°, worse than a random fit (i.e., 45°). The only place that local lithospheric thickness variation seems to match observation is in north-central NV, where a semi-circular pattern overlaps part of the observed larger circular SKS pattern. However, the predicted SKS splitting time in this region is much smaller than observed, casting doubt on the significance of this contribution.

3.2 Model 2: The subducting Juan de Fuca slab

Subducting slabs are usually considered to play an important role in forming mantle anisotropy and SKS observations (Long and Becker, 2010; Zandt and Humphreys, 2008; Hu et al., 2017). Slabs can influence mantle flow through both poloidal and toroidal flows (Long and Becker, 2010). The poloidal flow above a slab is perpendicular to the trench, and the toroidal flow, originating from below the slab to above around slab edges, usually forms a circular pattern (Stegman et al., 2006; Faccenda and Capitanio, 2013).

Model 2 is similar to that from Liu and Stegman (2011), except that a thick continental lithosphere is absent. This allows us to focus on the effect of the slab, as usually done in idealized subduction simulations (e.g., Faccenda and Capitanio, 2013). In this model, the Juan de Fuca slab deforms and segments during subduction (Fig. 4a, 4b). The continental mantle has a dominant poloidal flow induced by subduction, and the two major slab segments span a largely uniform SW-NE flow field at 200 km depth (Fig. 4a), while the oceanic mantle still follows the typical Couette flow, as in Model 1. Below the western U.S., there is some local disturbance of mantle flow around the slab pieces at depths (Fig. 4). In the cratonic mantle, the flow is more uniform and gets less influence from the slab.

Thus calculated mantle LPO demonstrate many prominent features, in contrast to those from Model 1. First, the overall anisotropy magnitudes are larger (Fig. 4c-d). Second, the oceanic mantle's OFAs are not just parallel to the plate motion anymore (Fig. 4c-d). Both reflect enhanced mantle deformation at depths due to the presence of the slab. Most of the OFA patterns at depth follow that of the mantle flow, due to its relatively simple geometry. Some local semi-circular patterns develop close the slab, such as those in western NV and central CA.

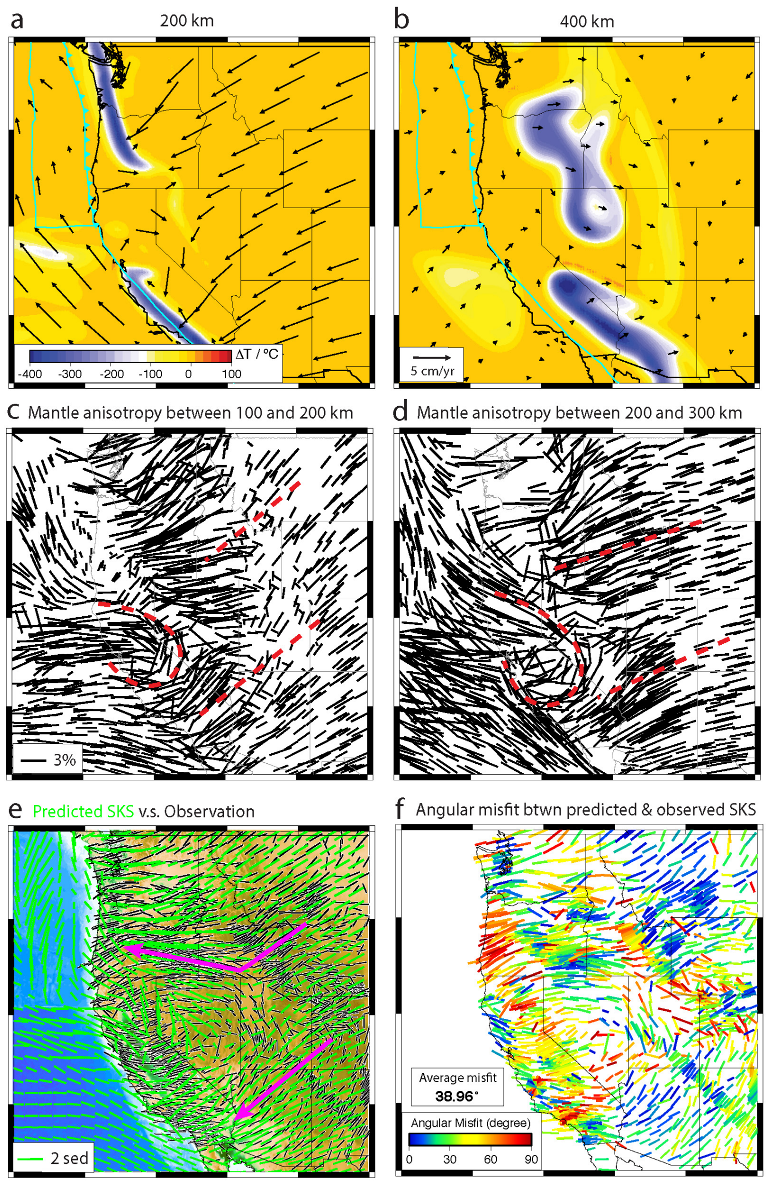

Figure 4: Same as Figure 3 but for Model 2. Red dashed lines delineate key anisotropy features. Magenta arrowed lines in (e) delineate the mantle flow unique for this model. The magnitude of predicted SKS splitting is stronger than that in Model 1.

Due to the relatively simple anisotropy patterns, the depth-integrated SKS prediction also largely matches mantle flow (LPO) for most of the regions (Fig. 4e). For example, the oceanic region sees a dominant pattern of plate motion, and the continental mantle is mostly slab-driven poloidal flow. Close to the coast, some deviation occurs, but a clear circular pattern is missing, and the predicted SKS does not correlate with the observed SKS pattern. In this model, flow-induced SKS splitting below the stable cratonic region matches that observed, contributing to an apparent good fit with an average of 39° misfit (Fig. 4f). This match, however, does not necessarily validate the mantle flow, which also requires an explanation of other processes as discussed later.

3.3 Model 3: Active subduction + lithosphere structure

Model 3 includes both the subducting Juan de Fuca slab and the seismically imaged continental lithosphere (Fig. 2), allowing examination of their joint effects in modulating mantle flow (Fig. 5a, 5b). Another difference from Model 2 is that we infer the geometry of the Juan de Fuca slab at 20 Ma using the hybrid inversion approach (Zhou and Liu, 2017) instead of from a pure forward simulation since 40 Ma (Liu and Stegman, 2011). This results in a better match to the observed mantle seismic structure, especially that the slab dip angel decreases due to enhanced hydrodynamic suction from the upper plate (e.g., Hu et al., 2016). At present, down to 200 km, the southern edge of the slab is surrounded by a strong toroidal flow (Fig. 5a). Both this toroidal flow and the sinking of the slab in the Pacific Northwest draws the mantle flow northward from southern B&R. The existence of a thick cratonic lithosphere to the east couples the asthenosphere flow with the plate motion, in contrast to the slab-induced return flow in Model 2 (Fig. 4a).

In the oceanic region, the OFA pattern is similar to that in Model 2. In the continental region, the varying thickness of the continental lithosphere exerts a strong influence

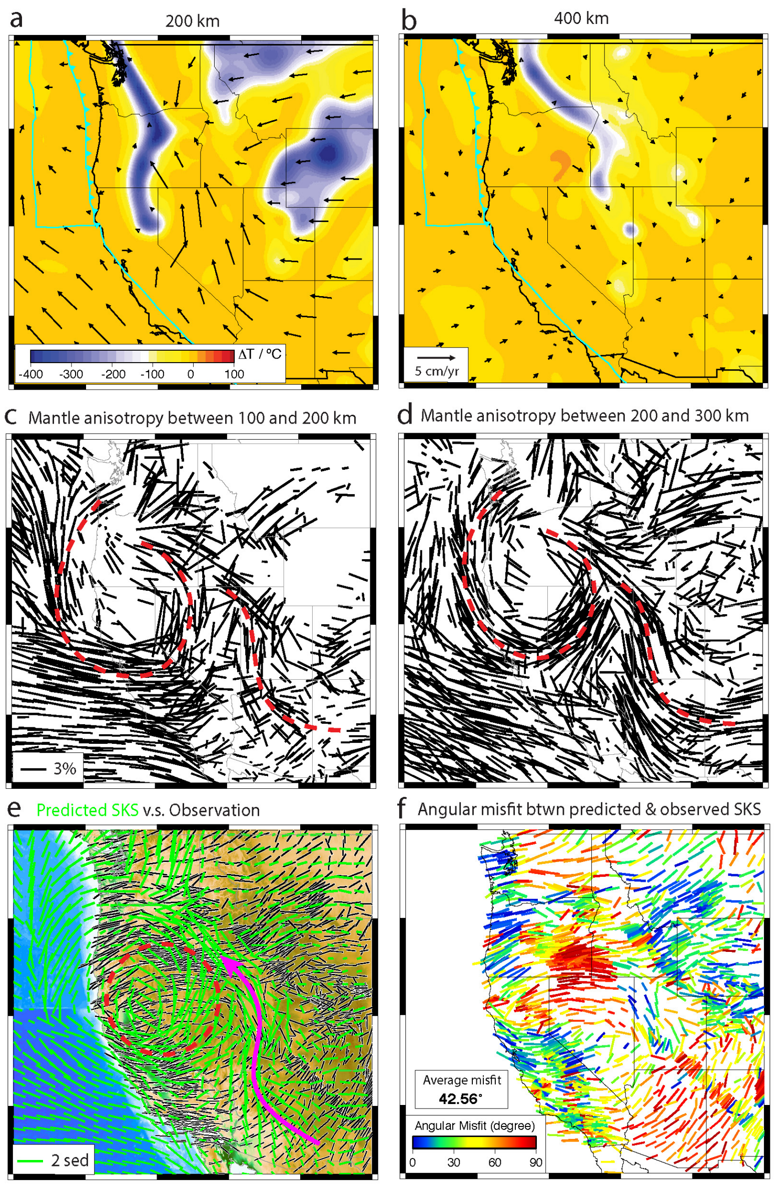

Figure 5: Same as Figure 3 but for Model 3. A circular SKS pattern is predicted in the right location as observed, but many details are off, with notable regions being the southern B&R and the Pacific Northwest.

on the distribution of OFA. There is a clear east-to-west contrast of OFA across the lithospheric step (Fig. 5c-5d), where the eastern part has relatively simple plate-motion parallel orientation, while the western part displays more complex patterns. A strong and broad circular anisotropy pattern develops over the region covering OR, CA and NV, as is due to the toroidal flow below and around the southern slab edge (Fig. 5c, 5d). The OFA direction in the southern B&R is largely parallel to the northwestward mantle flow.

The resulting SKS prediction differs from Model 2 in that the areas with large SKS splitting occupy most of the regions to the west of the lithospheric step (Fig. 5e-f). The predicted rotating SKS pattern becomes wider and more circular, close to observation. The strong SKS splitting in eastern NV, western Utah (UT), and central CA matches observation well. The enhanced SKS splitting within easternmost SRP also better matches observation. However, predictions within other regions are still off. In particular, the SKS orientation in eastern OR, northern NV and southernmost B&R is almost orthogonal to observation, significantly decreasing the average angular misfit to ~43° (Fig. 5f).

3.4 Model 4: Model 3 + ancient Farallon slab

Models 1 – 3 miss many tomographic features imaged below central-eastern U.S., especially the large number of fast anomalies below the east coast (Fig. 2; Sigloch, 2011; Schmandt and Lin 2014), traditionally interpreted as the ancient Farallon slab (e.g., Grand et al., 1997). By converting this ancient slab pile into positive density anomalies, the mantle flow differs again from that in previous models. Below the western U.S., the mantle flow becomes predominantly eastward (Figures 6a, 6b), instead of being westward as most other models show. This eastward flow component reflects the viscous drag from the sinking of the ancient Farallon slab (Figure S1; Zhou et al., 2018). Both a map and a cross-sectional view of this flow field change are shown in Figure S1, where we compare the results from Model 3 and 4; both these models further include hot anomalies in order to track the mantle evolution. We emphasize that the presence of hot anomalies do not change the flow direction in most places (Zhou et al., 2018), as also discussed in the next section.

The anisotropy pattern changes greatly as well, compared to the previous models (Figure 6c-d). Due to the eastward flow component in southern B&R, the OFA orientation switches to more E-W direction at all depths. This starts to outline a circular pattern largely centered in western Nevada. More variations appear below the craton. The OFA orientation around the Juan de Fuca slab changes rapidly over depth, but with both the pattern and intensity extending eastward, indicating the effect of the ancient Farallon slab.

The resulting SKS splitting shows additional improvements (Fig. 6e-f) from that in Model 3 (Fig. 5). The predicted circular pattern expands further east to central UT, similar to that observed. In the southern B&R, the modeled SKS splitting is now oriented NE-SW, consistent with both the underlying anisotropy and the observed SKS orientation. The SKS prediction along the SRP and eastern B&R, due to flow around the craton edges (Fig. 6a, 6e), further matches observation. However, there are still some mismatches. In California, the predicted fast direction is more N-S than that observed. The prominent E-W fast splitting in southern Oregon and Idaho is not yet predicted. The average angular misfit reduces to ~40° (Fig. 5f).

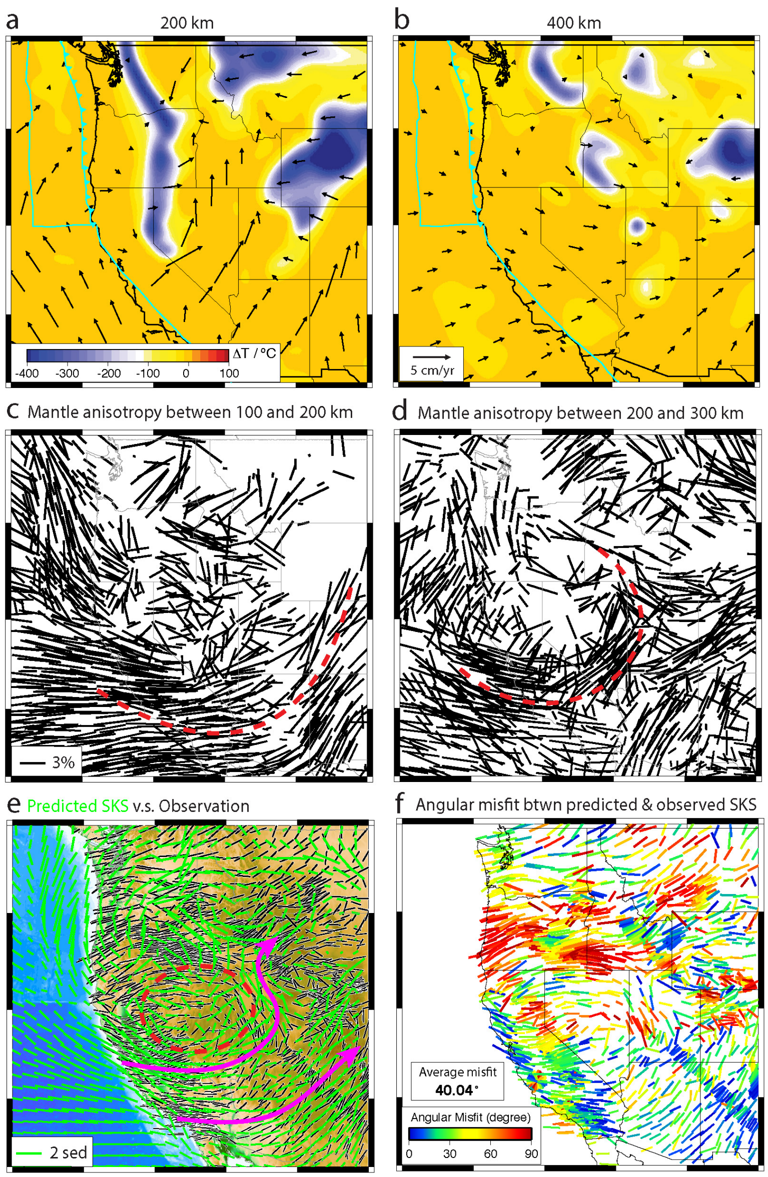

Figure 6: Same as Figure 3 but for Model 4. The predicted circular pattern expands further east relative to that in Model 3. The match is the southern B&R is significantly improved, due to the enhanced eastward mantle flow.

3.5 Model 5: Model 4 + hot asthenosphere anomalies

The last geodynamic component we further consider is hot mantle anomalies that are widespread throughout the upper mantle below the western U.S. Zhou et al. (2018) proposed that most of these shallow hot anomalies originated from the Pacific upper mantle since the mid-Miocene. The intrusion of this hot mantle below the sites of intra-plate volcanism is facilitated by, on one hand, dynamic pressure below the Juan de Fuca plate and, on the other hand, the sinking of the ancient Farallon slab further east.

Since the buoyant and weak hot anomalies would affect mantle flow at upper mantle depths, the pattern of mantle anisotropy would change accordingly. The low viscosity of the hot mantle decouples surface plate motion from the mantle below. Therefore, the mantle flow in the oceanic region, especially beneath the Juan de Fuca plate, deviates locally from the plate motion direction, with the oceanic asthenosphere flows largely westward (Fig. 7a). The present-day mantle velocities below the western U.S. are similar to those in Model 4, mostly going eastward, although with increased magnitudes at asthenospheric depths. However, the presence of hot anomalies affects the slab geometry and mantle flow below the Pacific Northwest, where a localized E-W deformation pattern persists around the center of the tearing slab (Fig. 8).

The anisotropy patterns further evolve (Fig. 7c-d) relative to Model 4. Most prominently, the circular pattern is further enlarged to the east and north and is now centered at western NV and northern CA. Such an OFA pattern represents the best prediction among all models discussed here. To the north, in OR and ID, a strong E-W oriented OFA structure is developed for the first time among all models, controlled by the enduring eastward intrusion of the hot mantle along the SRP since mid-Miocene (Figs. 2, 7; Zhou et al., 2018). On the west, in California, the predicted OFA forms a more coherent rotating pattern compared to other models, forming the western portion of the large anisotropy swirl.

The resulting SKS splitting pattern in this model could match most key observational aspects (Fig. 7e). The E-W oriented strong SKS splitting in OR and ID is consistently reproduced. This trend continues along the SRP into northern WY, best matching observation. A similarly strong stream of N-S oriented SKS in eastern NV and western UT along the craton edge merges northward with that along the SRP. Together with the smoothly transitioning and rotating SKS pattern to the west and south of NV, a regional-scale circular pattern of SKS splitting forms, best mimicking that observed.

Some local discrepancies still exist. These include the small offset of the center of the large circular pattern in northern NV, the southeastern edge of the circle in Arizona, as well as regions near the Canada-U.S. and U.S.-Mexico borders where the tomography image starts to lose resolution. Even with these local offsets, the average angular misfit drops significantly down to ~33° (Fig. 6f), which represents the bestfit among all models presented. As discussed later, these small-scale features are sensitive to model details that are not well constrained given the amount of data assimilated in these models.

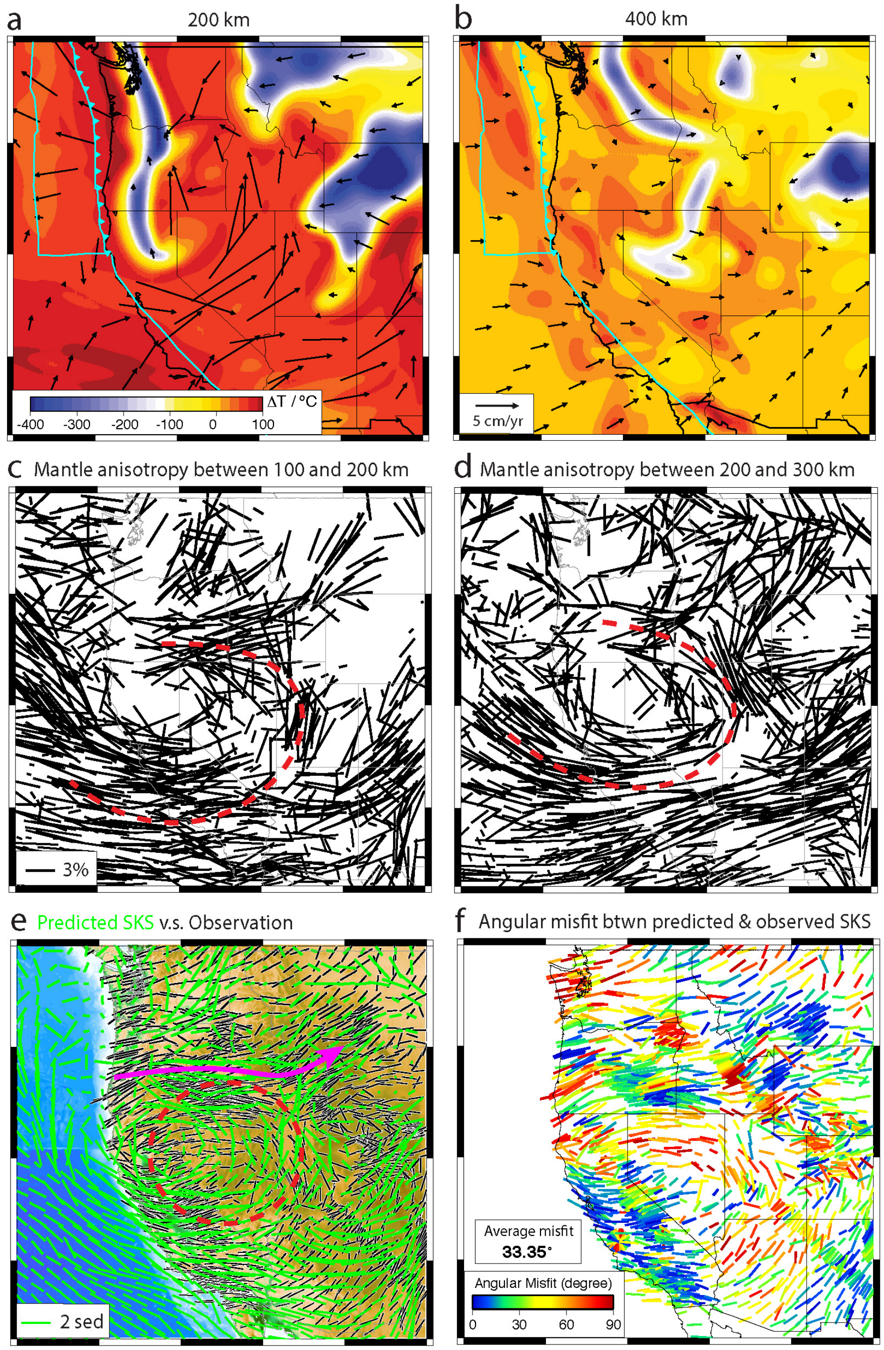

Figure 7: Same as Figure 3 but for Model 5. This model, among all cases, best matches the key SKS features. Relative to Model 4 (Figure 6), the observation in the Pacific Northwest is significantly improved, due to the intruding hot mantle below the region.

3.6 Temporal evolution of mantle anisotropy

Based on the best-fit model (Model 5), we also examine the temporal development of SKS splitting by overplotting the evolving SKS pattern on the temperature field at 200 km depth (Fig. 8a-e). Tests show that the observed SKS data could be best reproduced by considering mantle deformation since 10 Ma. A rotating pattern starts to form around the central NV lithospheric drip as early as 8 Ma (Fig. 8a). The fast direction along OR-SRP comes into shape by 6 Ma (Fig. 8b), where the magnitude of SKS splitting grows larger. Over subsequent times, the anisotropy pattern remains stable while the amplitude steadily increases (Fig. 8 c-e).

In another test, we assume the present-day mantle flow has remained unchanged since 10 Ma (Model 6), and use this steady flow to train the mantle fabric. The resulting SKS prediction (Fig. 8f) is remarkably similar to the case with the time-dependent flow. This reinforces that the flow pattern during the past 10 Ma is largely stable.

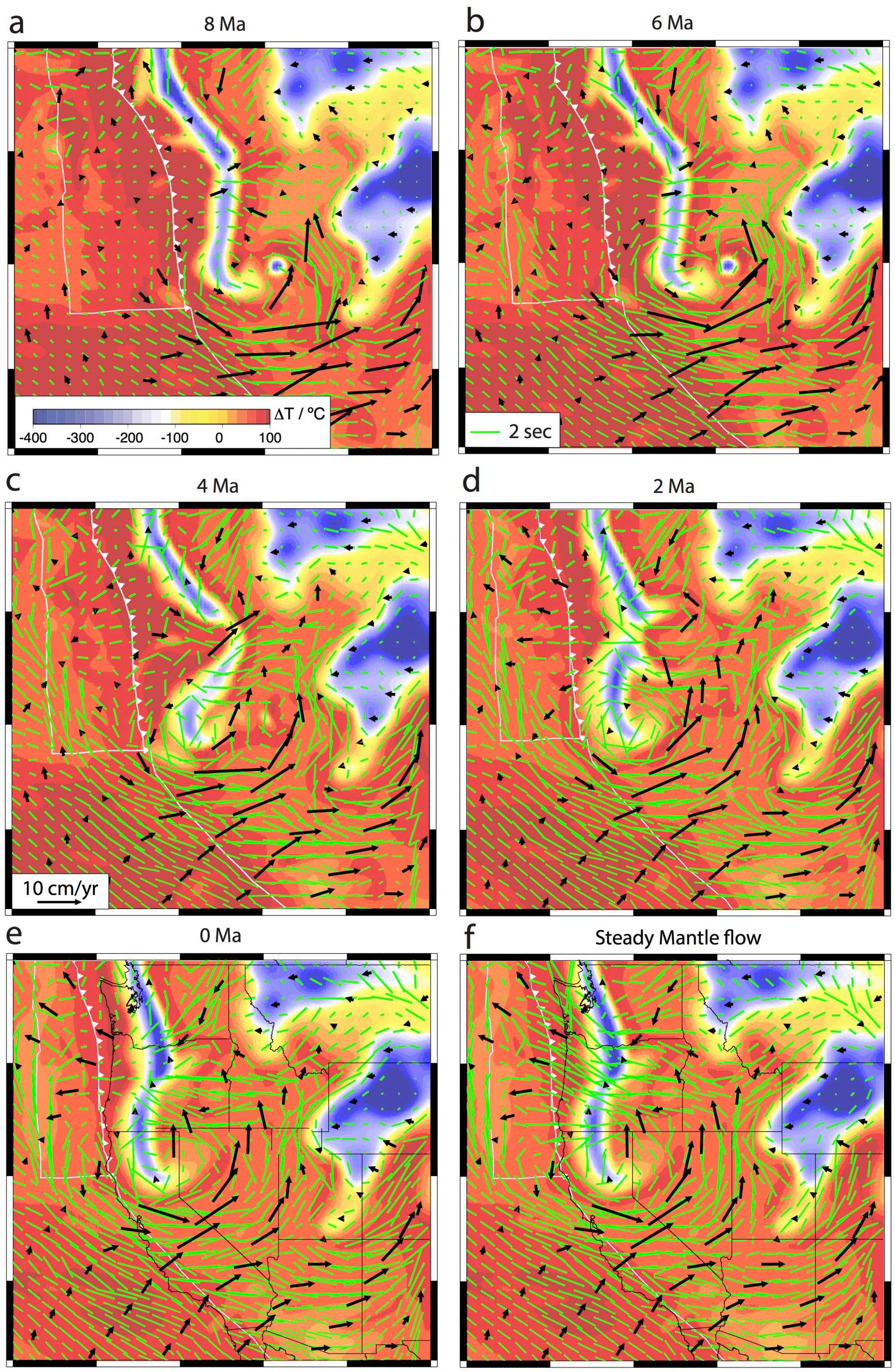

Figure 8: Temporal evolution of mantle flow and the resulting SKS pattern. (a-e) Prediction during the past 10 Ma based on the evolving mantle flow from Model 5. (f) Predicted present-day SKS pattern assuming a fixed pattern of present-day mantle flow since 10 Ma. Temperature at 200 km is plotted as the background. The predicted SKS patterns remain similar over time while the magnitude steadily grows stronger.

4. Discussion

In this study, we focus on reproducing the SKS observation over the tectonically active western U.S. Although the complex underlying dynamics poses a major challenge to numerical modeling, the observed anisotropy should mostly reflect recent mantle deformation with little contribution from fossil fabrics as commonly observed within the table continental lithosphere. Therefore, we neglect the effect of lithospheric fossil anisotropy (assuming above 100 km depth) in these calculations.

From the models presented above, we find that the SKS splitting data requires a proper simulation of an array of complex mantle structures and their associated mantle flow over time (e.g., Fig. 2). In contrast, none of the previously proposed conceptual models will suffice to explain all the anisotropy observations in the tectonically active western U.S. The data assimilation nature of our models allows a step-by-step analysis for the driving mechanisms of the mantle flow and resulting anisotropy, as well as the relevance of previously proposed models.

The modulation of mantle flow by lithosphere thickness variation is indeed an intuitive mechanism, but its effect seems to be restricted to the vicinity of the assumed lithosphere variations, including both the central-NV drip and the cratonic edge near the Rockies (Figs. 3-7). The fact that the western U.S. represents a subduction zone suggests that oceanic slabs must play an important role, and this notion is consistently confirmed in this study (Figs. 4-7). However, the exact deformation history and mantle flow evolution associated with these slabs have remained as the greatest challenge in geodynamic modeling. This is also the reason for carrying out the simulation exercises in Model 2 through Model 5.

A single slab sinking into a freely deforming mantle is a straightforward way to picture the 3D configuration of subduction (Stegman et al., 2006; Schellart et al., 2007). However, such a model with the observed subduction history (Model 2) only predicts a broad westward returning flow and a smooth anisotropy pattern (Fig. 4). This model does not predict a large-scale circular pattern of anisotropy due to toroidal flow around the slab edge, as Zandt and Humphreys (2008) proposed. This calls on the need of other tectonic mechanisms, such as realistic geometry of the overriding plate, which has been shown to affect slab evolution (Capitanio et al., 2011; Taramón et al., 2015; Hu et al., 2016). Model 3, therefore, combines the effects of the subducting slab and the continental lithosphere, and indeed better reproduces the circular anisotropy pattern as observed.

How former subducted slabs influence upper-mantle dynamics represents an outstanding question. Training mantle anisotropy using flow induced by deep mantle density anomalies (Model 4) makes a unique contribution to addressing this problem by showing that slabs subducted as early as 100 Ma are still actively affecting the shallow mantle. Although the ancient Farallon slab is already below the east coast, its impact on the upper mantle is still so significant that it switches the mantle flow direction below the western U.S. from being westward to become eastward (Figs. 5-7, S1). Thus generated flow further extends the region of strong SKS splitting to below the cratonic interior, and shifts the location of the circular pattern eastward to central

Nevada. This model basically establishes the overall pattern of the observed SKS splitting over western U.S., except for the Pacific Northwest.

Final inclusion of hot mantle anomalies in the model (Model 5) provides an improved fit to the E-W fast anisotropy in OR and ID (Fig. 7). This is the only place where the hot mantle actively changes mantle flow and anisotropy, since the extra heat increases the upper mantle dynamic pressure beneath the Juan de Fuca plate that allows the shallow slab tears to pump more material from the oceanic asthenosphere into the western U.S. upper mantle. The resulting strong shear deformation between the eastward moving sub-slab mantle (Figs. 7, 8) and the westward retreating mantle wedge (Fig. 7a) forms the prominent E-W anisotropy at the lower Pacific Northwest. For other regions, the presence of the low viscosity hot mantle mostly enhances local velocity, as seen from the eastward expanded flow region and anisotropy pattern.

We emphasize that these models, although already quite sophisticated, may not be able to uniquely constrain the origin of all local anisotropy features. This is because 1) the presented models all have uncertain input parameters, and 2) seismic anisotropy responds differently to different mantle structures. For example, in Model 3, if we replace the seismically imaged lithosphere with a parameterized geometry that approximates the NW-SE oriented lithosphere step (Fig. S2), the resulting SKS splitting pattern will differ significantly (Fig. 9a vs. Fig. 5): the circular pattern predicted in Model 3 (Fig. 5) largely vanishes, but the fit in OR-ID and southern B&R improves. This suggests that fine-scale lithosphere structures strongly affect local deformation. In another test based on Model 5, when we remove most of the hot mantle entering the southern B&R, the resulting SKS prediction remains largely unchanged (Fig. 9b), indicating an insensitivity to these dynamic structures. A similar result is observed if we further include the lower mantle plume in Model 5, implying its negligible role in modulating upper mantle deformation. In addition, we caution that estimating mantle flow from seismic anisotropy can be tricky: although there seem to be some similar anisotropy features between the two models in Figure 9a and 9b, their responding mantle flow directions below the western U.S. are actually opposite to each other.

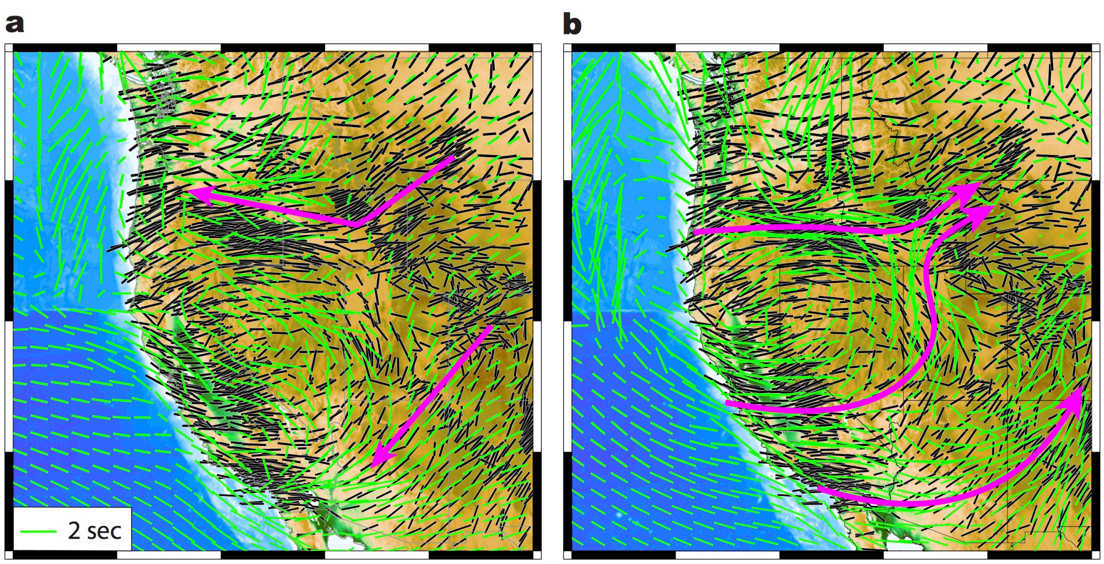

Figure 9: Two alterative scenarios of SKS prediction. (a) Same as Model 3 but with the seismically imaged lithosphere replaced by a parameterized one (Fig. S2), as that adopted in Liu & Stegman (2011). (b) Same as Model 5 but with a reduced amount of hot mantle entering the southern Basin & Range. Note the overall similar patterns to those based on their respective alternative models (Figures 5, 7).

Further uncertainties are related to the micro-flow simulations of the strain-induced LPO development, which have been calibrated against simple flows (simple shear and uniaxial shear) at low strains. As a result, the predicted anisotropy is able to well reproduce the SKS observations only when the mantle flow is sub-horizontal, while the fit degrades systematically in proximity of the trench where the slab-induced mantle flow has a strong vertical flow component (Faccenda and Capitanio, 2013; Hu et al., 2017), as is also observed in this study (e.g., Fig. 9b).

Importantly, this study may help to clarify on and reconcile the role of various mantle processes influencing the formation of Yellowstone-related volcanism during the late Cenozoic. A popular hypothesis is that these volcanic activities are directly generated from a mantle plume that is vertically rising below Yellowstone (e.g., Pierce & Morgan, 1992), a view that gains additional support from recent tomographic images (e.g., Schmandt & Humphreys, 2010; Nelson & Grand, 2018). However, a hot mantle transition zone below the region implied by a passing plume is recently challenged (Gao & Liu, 2015; Zhou, 2018). This study, together with our previous modeling efforts (Liu & Stegman, 2012; Leonard & Liu, 2016; Zhou et al., 2018), quantifies the various geodynamic processes that could have affected the evolution of the heat source behind the intraplate volcanism.

The bestfit model (Model 5) suggests that the eastwardly intruding Pacific hot mantle below Oregon determines the eastward flow toward Yellowstone; this flow pattern forms the prominent east-west SKS splitting along this corridor, a conclusion also reached in a recent local anisotropy study (Dave & Li, 2016). In contrast, other minor-in-volume hot anomalies including the plume itself (Fig. 2) have negligible effect in changing the local flow pattern (Figs. 6, 7; Zhou et al., 2018). The secondary-to-negligible role of the plume in modulating mantle flow implies a minor plume contribution to the overall heat source of the intraplate volcanic system. However, we note that the geochemistry of the volcanism likely requires a deep mantle contribution, an aspect the presented models are yet to explain. We suggest that future work is needed to further reconcile the lower mantle seismic image (e.g., Nelson & Grand, 2018), the transition zone thermal-chemical state (e.g., Zhou, 2018), and the upper mantle dynamics (e.g., Zhou et al., 2018; this study).

5. Conclusion

With a systematic evaluation on the resulting mantle flow of various mantle structures, this study outlines a detailed geodynamic configuration below the western U.S. with the following implications:

- The mantle flow is more complex than previous conceptual models suggested, due to the presence of multiple dynamic features.
- The observed seismic anisotropy represents a joint contribution from the active subducting Juan de Fuca slab, the east-west variation of lithospheric thickness, the descending ancient Farallon slab below the east coast, as well as the eastwardly intruding hot Pacific mantle through slab tears.
- The best-fit model further supports our recent notion that the Yellowstone volcanic system has been fueled mostly by heat from the shallow Pacific mantle instead of from the putative Yellowstone plume.

Acknowledgements: The numerical models were performed using CitcomS (www.geodynamics.org) and GPlates (www.gplates.org). Figures were prepared using the GMT software package (https://www.soest.hawaii.edu/gmt/). L.L. thanks NSF support through grants EAR-1345135 and 1554554. This research is part of the Blue Waters sustained-petascale computing project, which is supported by the National Science Foundation (awards OCI-0725070 and ACI-1238993) and the state of Illinois. Blue Waters is a joint effort of the University of Illinois at Urbana-Champaign and its National Center for Supercomputing Applications. This work is also part of the "PRAC Title 4-D Geodynamic Modeling With Data Assimilation: Origin Of Intra-Plate Volcanism In The Pacific Northwest" PRAC allocation support by the National Science Foundation (award number ACI 1516586). This work also used the Extreme Science and Engineering Discovery Environment (XSEDE), which is supported by National Science Foundation grant number ACI-1548562.

References:

Assumpção, M., Heintz, M., Vauchez, A., Silva, M.E., 2006. Upper mantle anisotropy in SE and Central Brazil from SKS splitting: evidence of asthenospheric flow around a cratonic keel. Earth Planet. Sci. Lett.250 (1), 224–240.

Becker, T. W., Schulte-Pelkum, V., Blackman, D. K., Kellogg, J. B., & O'Connell, R. J. (2006). Mantle flow under the western United States from shear wave splitting. Earth and Planetary Science Letters, 247(3-4), 235-251.

Becker, T. W., Lebedev, S., & Long, M. D. (2012). On the relationship between azimuthal anisotropy from shear wave splitting and surface wave tomography. Journal of Geophysical Research: Solid Earth, 117(B1).

Becker, T.W., Conrad, C.P., Schaeffer, A.J., Lebedev, S., 2014. Origin of azimuthal seismic anisotropy in oceanic plates and mantle. Earth Planet. Sci. Lett. 401, 236–250.

Beghein, C., Snoke, J. A., & Fouch, M. J. (2010). Depth constraints on azimuthal anisotropy in the Great Basin from Rayleigh-wave phase velocity maps. Earth and Planetary Science Letters, 289(3-4), 467-478.

Buehler, J. S., & Shearer, P. M. (2014). Anisotropy and Vp/Vs in the uppermost mantle beneath the western United States from joint analysis of Pn and Sn phases. Journal of Geophysical Research: Solid Earth, 119(2), 1200-1219.

Capitanio, F. A., Faccenna, C., Zlotnik, S., & Stegman, D. R. (2011). Subduction dynamics and the origin of Andean orogeny and the Bolivian orocline. Nature, 480(7375), 83.

Couvy, H., Frost, D. J., Heidelbach, F., Nyilas, K., Ungár, T., Mackwell, S., & Cordier, P. (2004). Shear deformation experiments of forsterite at 11 GPa-1400 C in the multianvil apparatus. European Journal of Mineralogy, 16(6), 877-889.

Dave, R., & A. Li (2016), Destruction of the Wyoming craton: seismic evidence and geodynamic processes, Geology, 44, 883-886.

Druken, K. A., Long, M. D., & Kincaid, C. (2011). Patterns in seismic anisotropy driven by rollback subduction beneath the High Lava Plains. Geophysical Research Letters, 38(13).

Durinck, J., Legris, A., & Cordier, P. (2005). Pressure sensitivity of olivine slip systems: first-principle calculations of generalised stacking faults. Physics and Chemistry of Minerals, 32(8-9), 646-654.

Faccenda, M., & Capitanio, F. A. (2013). Seismic anisotropy around subduction zones: Insights from three-dimensional modeling of upper mantle deformation and SKS splitting calculations. Geochemistry, Geophysics, Geosystems, 14(1), 243-262.

Fouch, M.J., Fischer, K.M., Parmentier, E.M., Wysession, M.E., Clarke, T.J., 2000. Shear wave splitting, continental keels, and patterns of mantle flow. J. Geophys. Res., Solid Earth 105 (B3), 6255–6275.

Foster, K., Dueker, K., Schmandt, B., Yuan, H., (2014). A sharp cratonic lithosphere–asthenosphere boundary beneath the American Midwest and its relation to mantle flow. Earth Planet. Sci. Lett. 402, 82–89.

Gao, S. S., and K. H. Liu (2015), Mantle transition zone discontinuities beneath the contiguous United States, J. Geophys. Res. Solid Earth, 119, 6452–6468, doi:10.1002/2014JB011253.

Hansen, S. M., Dueker, K., & Schmandt, B. (2015). Thermal classification of lithospheric discontinuities beneath USArray. Earth and Planetary Science Letters, 431, 36-47.

Hu, J., Liu, L., Hermosillo, A., Zhou, Q. (2016), Simulation of Late Cenozoic South American flat-slab subduction using geodynamic models with data assimilation, Earth Planet. Sci. Lett., 438, 1–13.

Hu, J., Faccenda, M., & Liu, L. (2017). Subduction-controlled mantle flow and seismic anisotropy in South America. Earth and Planetary Science Letters, 470, 13-24.

Huang, Z., & Zhao, D. (2013). Mapping P-wave azimuthal anisotropy in the crust and upper mantle beneath the United States. Physics of the Earth and Planetary Interiors, 225, 28-40.

Jung, H., & Karato, S. I. (2001). Water-induced fabric transitions in olivine. Science, 293(5534), 1460-1463.

Kaminski, E., Ribe, N. M., & Browaeys, J. T. (2004). D-Rex, a program for calculation of seismic anisotropy due to crystal lattice preferred orientation in the convective upper mantle. Geophysical Journal International, 158(2), 744-752.

Karato, S. I., and Wu, P. (1993), Rheology of the upper mantle: a synthesis, Science, 260 (5109), 771-778.

Karato, S. I., Jung, H., Katayama, I., & Skemer, P. (2008). Geodynamic significance of seismic anisotropy of the upper mantle: new insights from laboratory studies. Annu. Rev. Earth Planet. Sci., 36, 59-95.

Katayama, I., & Karato, S. I. (2006). Effect of temperature on the B-to C-type olivine fabric transition and implication for flow pattern in subduction zones. Physics of the Earth and Planetary Interiors, 157(1-2), 33-45.

Leonard, T. and Liu, L. (2016), The role of a mantle plume in the formation of Yellowstone volcanism, Geophys. Res. Lett., 43, doi:10.1002/2015GL067131.

Lin, F. C., Ritzwoller, M. H., Yang, Y., Moschetti, M. P., & Fouch, M. J. (2011). Complex and variable crustal and uppermost mantle seismic anisotropy in the western United States. Nature Geoscience, 4(1), 55.

Liu, L., & Gurnis, M. (2008). Simultaneous inversion of mantle properties and initial conditions using an adjoint of mantle convection. Journal of Geophysical Research: Solid Earth, 113(B8).

Liu, L., & Stegman, D. R. (2011). Segmentation of the Farallon slab. Earth and Planetary Science Letters, 311(1-2), 1-10.

Liu, L., and Stegman, D. R. (2012), Origin of the Columbia River flood basalt controlled by propagating rupture of the Farallon slab, Nature, 482, 386–390.

Long, M. D., & Becker, T. W. (2010). Mantle dynamics and seismic anisotropy. Earth and Planetary Science Letters, 297(3-4), 341-354.

Long, M. D. (2016). The Cascadia Paradox: Mantle flow and slab fragmentation in the Cascadia subduction system. Journal of Geodynamics, 102, 151-170.

McQuarrie, N., & Wernicke, B. P. (2005). An animated tectonic reconstruction of southwestern North America since 36 Ma. Geosphere, 1(3), 147-172.

Menke, W., & Levin, V. (2003). The cross-convolution method for interpreting SKS splitting observations, with application to one and two-layer anisotropic earth models. Geophysical Journal International, 154(2), 379-392.

Müller, R. D., Sdrolias, M., Gaina, C., & Roest, W. R. (2008). Age, spreading rates, and spreading asymmetry of the world's ocean crust. Geochemistry, Geophysics, Geosystems, 9(4).

Nelson, P. L. and Grand, S. P. (2018), Lower-mantle plume beneath the Yellowstone hotspot revealed by core waves, *Nature Geoscience*, doi:10.1038/s41561-018-0075-y.

Nikulin, A., Levin, V., & Park, J. (2009). Receiver function study of the Cascadia megathrust: Evidence for localized serpentinization. Geochemistry, Geophysics, Geosystems, 10(7).

Park, J., Yuan, H., & Levin, V. (2004). Subduction zone anisotropy beneath Corvallis, Oregon: A serpentinite skid mark of trench-parallel terrane migration?. Journal of Geophysical Research: Solid Earth, 109(B10).

Pierce, K. L., and Morgan, L. A. (1992), The track of the Yellowstone hotspot: Volcanism, faulting, and uplift, in Regional Geology of Eastern

Idaho and Western Wyoming, Mem., vol. 179, edited by P. K. Link, M. A. Kuntz, and L. B. Platt, pp. 1–53, Geol. Soc. Am., Denver, Colo.

Raterron, P., Amiguet, E., Chen, J., Li, L., & Cordier, P. (2009). Experimental deformation of olivine single crystals at mantle pressures and temperatures. Physics of the Earth and Planetary Interiors, 172(1-2), 74-83.

Rieger, D. M., & Park, J. (2010). USArray observations of quasi-Love surface wave scattering: Orienting anisotropy in the Cascadia plate boundary. Journal of Geophysical Research: Solid Earth, 115(B5).

Schellart, W.P., Freeman, J., Stegman, D.R., Moresi, L., May, D. (2007), Evolution and diversity of subduction zones controlled by slab width, Nature, 446, 308-311.

Schmandt, B., & Humphreys, E. (2010). Complex subduction and small-scale convection revealed by body-wave tomography of the western United States upper mantle. Earth and Planetary Science Letters, 297(3-4), 435-445.

Schmandt, B., & Lin, F. C. (2014). P and S wave tomography of the mantle beneath the United States. Geophysical Research Letters, 41(18), 6342-6349.

Shen, W., & Ritzwoller, M.H. (2016), Crustal and uppermost mantle structure beneath the United States, J. Geophys. Res., 121, 4306-4342.

Sigloch, K. (2011). Mantle provinces under North America from multifrequency P wave tomography. Geochemistry, Geophysics, Geosystems, 12(2).

Stegman, D.R., Freeman, J., Schellart, W.P., Moresi, L., May, D. (2006), Influence of trench width on subduction hinge retreat rates in 3 - D models of slab rollback, Geochem. Geophys. Geosyst., 7, Q03012.

Taramón, J.M., Rodríguez-González, J., Negredo, A.M., Billen, M.I. (2015), Influence of cratonic lithosphere on the formation and evolution of flat slabs: insights from 3-D time-dependent modeling, Geochem. Geophys. Geosyst., 16 (9), 2933–2948.

Vinnik, L.P., Makeyeva, L.I., Milev, A., Usenko, A.Y., 1992. Global patterns of azimuthal anisotropy and deformations in the continental mantle. Geophys. J. Int. 111 (3), 433–447.

West, J. D., Fouch, M. J., Roth, J. B., & Elkins-Tanton, L. T. (2009). Vertical mantle flow associated with a lithospheric drip beneath the Great Basin. Nature Geoscience, 2(6), 439.

Wagner, L. S., & Long, M. D. (2013). Distinctive upper mantle anisotropy beneath the High Lava Plains and Eastern Snake River Plain, Pacific Northwest, USA. Geochemistry, Geophysics, Geosystems, 14(10), 4647-4666.

Wagner, L. S., Fouch, M. J., James, D. E., & Long, M. D. (2013). The role of hydrous phases in the formation of trench parallel anisotropy: Evidence from Rayleigh waves in Cascadia. Geophysical Research Letters, 40(11), 2642-2646.

Wang, X., Ni, J.F., Aster, R., Sandvol, E., Wilson, D., Sine, C., Baldridge, W.S., (2008). Shear-wave splitting and mantle flow beneath the Colorado Plateau and its boundary with the Great Basin. Bull. Seismol. Soc. Am. 98 (5), 2526–2532.

Wüstefeld, A., Bokelmann, G., Barruol, G., & Montagner, J. P. (2009). Identifying global seismic anisotropy patterns by correlating shear-wave splitting and surface-wave data. Physics of the Earth and Planetary Interiors, 176(3-4), 198-212.

Yuan, H., & Romanowicz, B. (2010). Depth dependent azimuthal anisotropy in the western US upper mantle. Earth and Planetary Science Letters, 300(3-4), 385-394.

Zandt, G., & Humphreys, E. (2008). Toroidal mantle flow through the western US slab window. Geology, 36(4), 295-298.

Zhang, S., & Karato, S. I. (1995). Lattice preferred orientation of olivine aggregates deformed in simple shear. Nature, 375(6534), 774.

Zhong, S., McNamara, A., Tan, E., Moresi, L., & Gurnis, M. (2008). A benchmark study on mantle convection in a 3-D spherical shell using CitcomS. Geochemistry, Geophysics, Geosystems, 9(10).

Zhou, Q., & Liu, L. (2017). A hybrid approach to data assimilation for reconstructing the evolution of mantle dynamics. Geochemistry, Geophysics, Geosystems, 18(11), 3854-3868.

Zhou, Q., Liu, L., & Hu, J. (2018). Western US volcanism due to intruding oceanic mantle driven by ancient Farallon slabs. Nature Geoscience, 11(1), 70.

Zhou, Y. (2018), Anomalous mantle transition zone beneath the Yellowstone hotspot track, Nature Geoscience, doi: 10.1038/s41561-018-0126-4.